A Robust Adaptive Wavelet-based Method for Classification of Meningioma Histology Images

Hammad Qureshi[1], Nasir Rajpoot[1], Tim Nattkemper[2], and Volkmar Hans[3]

[1] Department of Computer Science, University of Warwick, UK
[2] Faculty of Technology, University of Bielefeld, Germany
[3] Institute of Neuropathogy, Evangelisches Krankenhaus, Bielefeld, Germany *

Abstract. Intra-class variability in the texture of samples is an important problem in the domain of histological image classification. This issue is inherent to the field due to the high complexity of histology image data. A technique that provides good results in one trial may fail in another when the test and training data are changed and therefore, the technique needs to be adapted for intra-class texture variation. In this paper, we present a novel wavelet based multiresolution analysis approach to meningioma subtype classification in response to the challenge of data variation. We analyze the stability of Adaptive Discriminant Wavelet Packet Transform (ADWPT) and present a solution to the issue of variation in the ADWPT decomposition when texture in data changes. A feature selection approach is proposed that provides high classification accuracy.

1 Introduction

Histology image analysis presents a new set of challenges to the scientific community. Histology images are real world data considerably different from synthetic textural data which is acquired using controlled procedures. Texture in histology images is non-stationary i.e. different areas in an image can have different textural properties which may represent different textural classes. Moreover, intra class variation amongst the samples belonging to the same class may be high and to make matters worse inter class differences amongst the samples may be low. This is true in the case of meningioma subtype images, as shown in Figure 1. Meningiomas account for about 20% of all brain tumours and exist in three different grades of malignancy (WHO Grade I-III), most being benign (over 80%) but some showing increased propensity to recurrence and malignancy. The problem of meningioma subtype classification essentially involves discriminating between four different subtypes of meningiomas. As can be seen in Figure 1, there can be large variation in the texture of images belonging to the same meningioma class. Moreover, there is also the problem of low inter-class differences amongst the texture samples. For instance, transitional resembles fibroblastic and fibroblastic resembles meningotheliamatous. This can be seen in the case of fibroblastic and meningiotheliamatous subtypes for first samples from left in (b) and (c) in Figure 1. This variation raises the issue of how a texture classification technique responds to the challenge of variability in texture samples belonging to the same textural class. A feature representation and extraction technique that works for

* Corresponding author's email address: hammad@dcs.warwick.ac.uk

one set of data may fail completely for another set. To resolve this issue for meningioma classification, we have taken up the Adaptive Discriminant Wavelet Packet Transform (ADWPT) proposed by Qureshi *et al.* [1] and improved it to resolve the problem of texture variation. The proposed method is more robust and at the same time produces higher accuracy results.

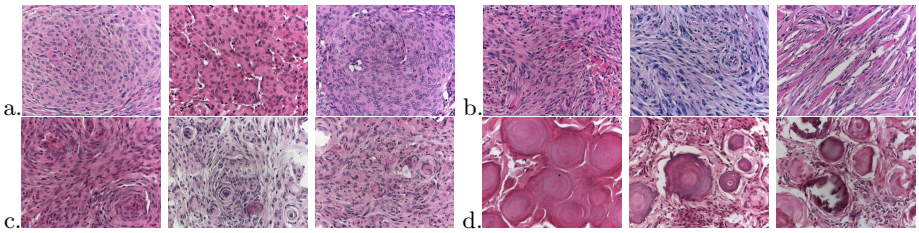

Fig. 1. Various Meningioma Images belonging to each subtype a. Meningiothelial, b. Fibroblastic, c. Transitional, d. Psammomatoes

Some work on meningioma subtype clustering was carried out by Lessman *et al.* [2], who described how self organizing maps can be combined with wavelet transforms for effective clustering of meningioma images. Qureshi *et al.* [1, 3] have performed classification of meningioma subtypes using the wavelet packets based ADWPT. Wirjadi *et al.* [4], on the other hand, perform classification between two meningioma subtypes using cell shape analysis. Shape and structural analysis of constituents of images has found wide application in histology image analysis [5]. Numerous segmentation techniques such as thresholding [6, 7], adaptive thresholding [8, 9], watershed algorithms [10], fuzzy clustering and active contours [11] have been used for the segmentation of nuclei and glands in histology images. But there are issues in using each of these techniques as thresholding tends to work better for uniform images and produces inconsistent results if the variability within the image sets is high as stipulated by Gurcan *et al.* [12]. Watershed algorithms tend to suffer with the same problem. Active contours deal better with the variability but multiple overlapping objects pose a difficult challenge for active contours as they may be enclosed to form one object. As can be seen from the images in Figure 1, meningioma images suffer from all the issues mentioned above. There is considerable variation within the texture samples and overlapping of structural components is frequent as can be seen for meningiothelial and psammomatous samples. Furthermore, the high intra-class variation and low inter-class variation would pose serious issues for any segmentation technique as the segmented constituents would differ greatly for different image samples belonging to the same class. On the other hand, techniques such as cell graphs [13], gray-level co-occurrence matrices [14, 15], Fourier transforms [16], wavelet transforms [2, 17], multi-wavelets [18] and fractal geometry [19–21] have found application in the domain of histology image classification. Classification algorithms based upon these techniques aim to perform a holistic structural or textural analysis of histology images rather than constituent parts obtained using segmentation, just as ADWPT does.

As indicated earlier, we aim to solve this problem of texture variation by employing the adaptive wavelet based analysis approach developed in [1, 3] and improve it so that it is robust to inter and intra-class variation. The advantage accrued from a multi-resolution analysis is that it helps in resolving the issue of texture complexity by decomposing the texture at multiple spatial and frequency resolutions. This implies that each subband in a wavelet decomposition represents different textural characteristics in terms of the spatial frequency content at a particular spatial resolution. Another interesting property of wavelet subband decomposition is that it produces sparse representations which get sparser after every level of filtering. High magnitude coefficients in an otherwise sparse subband correspond to presence of specific high frequency content in the corresponding image. These high frequency coefficients in a subband as a group form textural features that may correspond to textons [22]. As we shall soon see, this localization of features in various subbands using ADWPT will aid in achieving high classification accuracies. The ADWPT analyzes a histological image at various scales and spatial resolutions, as depicted in Figures 2 and 3 in Section 2.3, in the same way as neuropathologists carry out their analysis using a microscope. It determines the spatial resolutions which are most useful for analyzing a histology image and identifies them as the most discriminant subbands.

In this paper, we investigate the stability of the ADWPT and explore as to how it responds to the challenge of data variation. If there is a lack of stability in the decompositions produced then spatial frequency resolutions that are most useful may not be identified and hence the features that are optimal for classification of image subtypes may not be found. We resolve this issue by acquiring the most stable subbands. An estimate of how often a subband is decomposed, when the data changes, is obtained and only those subbands are selected which are decomposed more frequently. We show that the most stable subbands, i.e. subbands that are selected most often, produce the best results. We also introduce Fisher's discriminant as the distance function of choice for selecting the most discriminant subbands. Subband selection using Fisher's discriminant as the distance function in the algorithm in Section 2.3 produces better classification results.

2 The Classification Algorithm

In order to acquire an ADWPT-based representation, a series of steps must be carried out. The computation of ADWPT involves the following steps:

1. Acquire a Full Wavelet Packet Transform (FWPT) for each image in the texture sample.
2. Compute Multi-resolution Wavelet based Texture Templates (MWTT) for each texture class.
3. Determine discrimination power of each subband in MWTT and then perform subband selection based upon the discrimination power of a subband.

2.1 Full Wavelet Packet Transform (FWPT)

A full wavelet packet transform is simply the wavelet transform of both the low and high pass subbands at all levels. A wavelet transform for an image or 2-D

signal is carried out with a scaling function (low pass filter) $\Phi(x, y)$ and three wavelet functions $\Psi^i(x, y)$, where $i = 1, 2, 3$, which may be represented as,

$$\Phi(x, y) = \phi(x) * \phi(y), \tag{1}$$

$$\Psi^1(x, y) = \phi(x) * \psi(y), \Psi^2(x, y) = \psi(x) * \phi(y), \Psi^3(x, y) = \psi(x) * \psi(y), \tag{2}$$

where ϕ represents the scaling function and ψ represents the wavelet function. $\Psi^1(x, y)$ and $\Psi^2(x, y)$ perform wavelet filtering in one direction and scaling in another leading to horizontal and vertical details, whereas $\Psi^3(x, y)$ leads to the diagonal detail with wavelet filtering in both directions. The approximation and three detail subbands would then be given by,

$$\mathcal{W}_{d+1,2p,2q} = \Phi * \mathcal{W}_{d,p,q} \tag{3}$$

$$\mathcal{W}_{d+1,2p+1,2q} = \Psi^1 * \mathcal{W}_{d,p,q} \tag{4}$$

$$\mathcal{W}_{d+1,2p,2q+1} = \Psi^2 * \mathcal{W}_{d,p,q} \tag{5}$$

$$\mathcal{W}_{d+1,2p+1,2q+1} = \Psi^3 * \mathcal{W}_{d,p,q} \tag{6}$$

where d represents the depth of the wavelet tree and p, q are the frequency indices of the subband. $\mathcal{W}_{0,0,0} = I$ and corresponds to the image being analyzed. All subbands are decomposed to produce further approximation and detail subbands up to a predefined level J to produce a full wavelet packet transform (FWPT) and the FWPT tree is then pruned in a bottom-up fashion to obtain the most discriminant representation, as described in Section 2.3.

2.2 Multi-resolution Wavelet Texture Templates (MWTT)

Multi-resolution Wavelet Texture Templates (MWTTs) are obtained using a pseudo-averaging of the psuedo-probability density estimates (ppde) of a particular subband across all the training samples of a particular class. The ppde of a subband is given by,

$$s_{d,p,q}(m, n) = x^2_{d,p,q}(m, n) / \sum_{i=0}^{M-1} \sum_{j=0}^{N-1} x^2_{d,p,q}(i, j) \tag{7}$$

where $x_{d,p,q}(m, n)$ is the coefficient at location (m,n) in the subband $\mathcal{W}_{d,p,q}$ of size $M \times N$ at depth d and location p, q. The MWTT is computed by iteratively taking the pairwise average of the ppde of the same subband for all training images. It is important to note that these are computed for each class separately,

$$\mathcal{A}^{a_2}_{d,p,q}(m, n) = \frac{s^{a_1}_{d,p,q}(m, n) + s^{a_2}_{d,p,q}(m, n)}{2}, \qquad i = 2 \tag{8}$$

$$\mathcal{A}^{a_i}_{d,p,q}(m, n) = \frac{\mathcal{A}^{a_{i-1}}_{d,p,q}(m, n) + s^{a_i}_{d,p,q}(m, n))}{2}, \qquad i = 3 \ldots N_a \tag{9}$$

where $s^{a_i}_{d,p,q}(m, n)$ is the (m, n)th value of the ppde of a subband $\mathcal{W}_{d,p,q}$ for the image a_i belonging to class a and N_a is the number of training samples available for texture class a. The process is repeated for all subbands of the FWPT. It is important to note that an average of two subbands is computed

per iteration. The objective is to acquire a basic model of probability density values for each class so that differences between the classes can be estimated. The averaging mechanism is referred as pseudo-averaging as it is different from standard averaging. Pseudo-averaging is done to account for any sudden rise or fall in the probability density estimates. Figure 2 shows some subbands of the MWTTs obtained using the pseudo-averaging approach. It must be noted here that due to the high intra-class variability in the textures and the dependence of MWTTs on the images being used, the templates change with the data. These templates help in overcoming the problem of data variation because the FWPT produces sparse representations with textural data localized both in space and frequency. Hence, the textural data is decorrelated i.e. filtered into various domains with low frequency and high frequency content found separately in different subbands. We use these subbands to estimate the occurrence of useful textural features over the sample space using the pseudo-averaging of the ppdes describe above. The MWTT is an estimate of the textural characteristic represented by a subband over the entire sample space for a textural class. Some of the template subbands at various decomposition levels are shown in Figures 2 and 3.

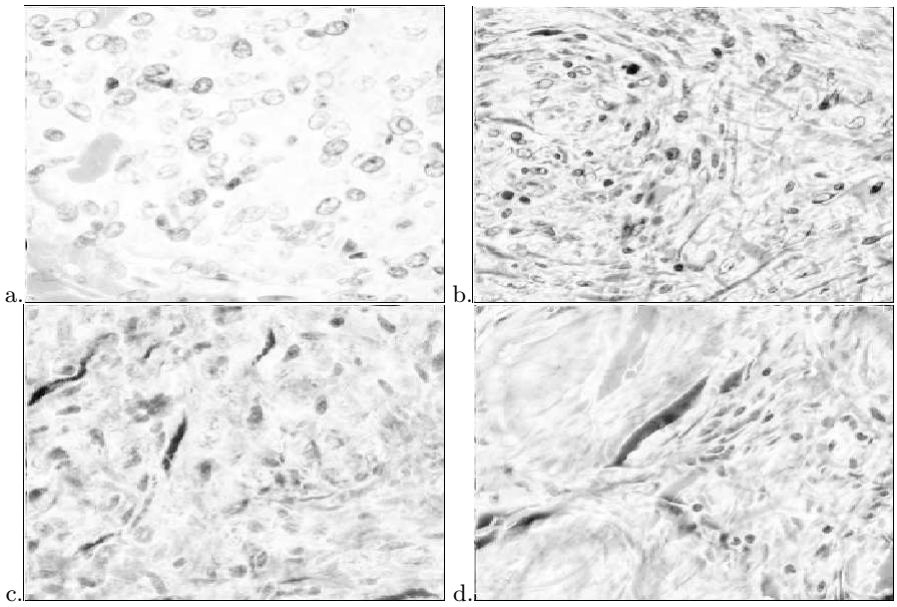

Fig. 2. Texture templates obtained using psuedo-averaging of subbands at a higher spatial resolution for training samples of a. Meningiothelial b. Fibroblastic c. Transitional d. Psammomatous Meningioma

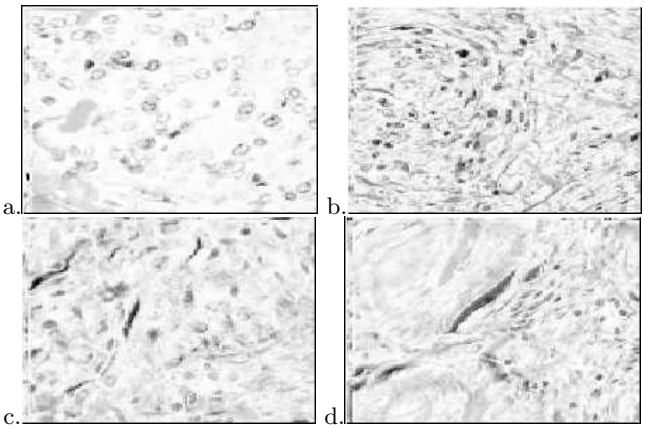

Fig. 3. Texture templates obtained using psuedo-averaging of subbands at a lower spatial resolution for training samples of a. Meningiothelial b. Fibroblastic c. Transitional d. Psammomatous Meningioma

2.3 Best Basis Selection based upon Discrimination Power of a Subband

The calculation of the most discriminant decomposition is of paramount importance for wavelet packets basis selection. This is acquired by using the sum of pairwise distances between MWTTs for all texture classes as an objective function and then selecting the subbands with a higher value using dynamic programming [23]. The Fisher distance $\mathcal{D}$ is used for the purpose which is a departure from the work of Qureshi *et al.* [1] who have preferred using Hellinger distance. The Fisher distance between two MWTTs for classes a and b can be computed as follows,

$$\mathcal{D}^{a,b}_{d,p,q} = \frac{(\mu^a_{d,p,q} - \mu^b_{d,p,q})^2}{(\sigma^a_{d,p,q})^2 + (\sigma^b_{d,p,q})^2} \tag{10}$$

where $\mu^a_{d,p,q}$ and $\mu^b_{d,p,q}$ represent the mean of the MWTT subband $\mathcal{W}_{d,p,q}$ for classes a and b and $\sigma^a_{d,p,q}$ and $\sigma^b_{d,p,q}$ represent the variance of the MWTT subband $\mathcal{W}_{d,p,q}$ for classes a and b respectively. Fisher distance is very different from Hellinger as it does not compute the difference between individual values of a subband but uses the statistical properties of the corresponding MWTTs representing each texture class to determine the discrimination power of a subband. As we shall soon see, the decompositions obtained using Fisher distance generate much better results compared to those produced by the Hellinger distance. The overall discrimination power $\mathcal{P}_{d,p,q}$ may be computed by,

$$\mathcal{P}_{d,p,q} = \sum_{(a,b)\in O} \mathcal{D}^{a,b}_{d,p,q} \tag{11}$$

where O is the set containing all the pairwise class combinations of the 4 different classes ($|O| = 6$) for subband $\mathcal{W}_{d,p,q}$. The process is repeated for all the

corresponding MWTT subbands at various levels. The algorithm for the best basis selection is given below.

1. Compute the J-level FWPT as described in Sec. 2.1 for each texture class.
2. Compute the MWTTs for all subbands and for all classes using (7)-(9).
3. Calculate the discrimination power $\mathcal{P}_{d,p,q}\ \forall\ d,p,q$ using (11).
4. Initialize $d = J-1$.
5. For all $0 \leq p < 2^d$, $0 \leq q < 2^d$, do the following:
   5a. If $\mathcal{P}_{d,p,q} < max[\mathcal{P}_{d+1,2p,2q}, \mathcal{P}_{d+1,2p,2q+1}, \mathcal{P}_{d+1,2p+1,2q}, \mathcal{P}_{d+1,2p+1,2q+1}]$ Keep the four child subbands at depth $d+1$ where $\mathcal{P}_{d,p,q}$ represents the discrimination power of a node at position p,q and depth d
   5b. Otherwise keep the parent at depth d and remove the child subbands.
6. Decrement d by 1.
7. If $d < 0$, then stop, otherwise goto step 5.

3 Stability of ADWPT

The meningioma histology image data is composed of a total of 960 images for 4 meningioma subtypes with 5 different patients per subtype. The sample data is identical to the one used by Qureshi *et al.* in [1, 3] with the difference being only in the way how the original data is divided. We divide the original image data of 1300×1030 in blocks of 512×512 and move the sampling window by 256 pixels first in the horizontal direction and then in the vertical direction. After each increment a subimage of 512×512 is extracted from the original image. Out of the original 4 images per patient, a total of 48 images are produced.

We select 4 patients from each subtype, leaving one out, and use them for MWTT construction. The process of computation of a decomposition for each test trial containing 4 different patients is carried out. 256 different combinations of patient's data using leave-one-out method are used to produce 256 ADWPT decompositions. These decompositions are combined to produce a union decomposition, such as the one shown in Figure 4. This union decomposition contains all the subbands that are ever decomposed for the distance function and the given test-trial data. The process of union of basis $\mathcal{B}$ from various test-trials is given by,

$$\mathcal{F}^* = \bigcup_{i=1}^{N_\mathcal{B}} \mathcal{B}_i^* = \mathcal{B}_1^* \bigcup \mathcal{B}_2^* \bigcup \ldots \mathcal{B}_{N_\mathcal{B}}^* \tag{12}$$

where $N_\mathcal{B}$ is the total number of ADWPT decompositions obtained for a given trial and $\mathcal{B}_i^*$ is the ith ADWPT. The decompositions obtained using the above methodology are often similar, but sometimes they differ significantly. The Fisher distance in (10) produces a total of 16 different and unique decompositions. We obtain a measure of stability for each subband decomposed in terms of the probability of it being decomposed in a test-trial run. The stability of a subband is computed as,

$$\mathcal{S}_{d,p,q} = N_{d,p,q}/N_T \tag{13}$$

where $N_{d,p,q}$ is the total number of times, the subband $\mathcal{W}_{d,p,q}$ is found in the decompositions produced for the various trial runs using different patient's data

combinations. N_T is the total number of trial runs which is equal to 256. A high value of $\mathcal{S}_{d,p,q}$ means that the subband is consistently regarded by the basis selection part of the algorithm (Section 2.3) as being discriminant and also robust as it is less likely to be highly dependent on the variation in data and texture samples. The decomposition showing stability values $\mathcal{S}_{d,p,q}$ for each subband is given in Figure 4.

In Figure 4, the stability $\mathcal{S}_{d,p,q}$ of all subbands is shown which is given in the magenta colour whereas the cyan colour denotes the standard deviation of its frequency of occurrence. As can be seen from Figure 4, many subbands have a high frequency of occurrence but there are some which can be seen to be less robust. The subbands with low stability values impact the classification accuracy in a negative manner. We will see in the results section that discarding less frequent subbands produces better results. The colour of the subband indicates its discrimination power. The lighter the colour the more discriminant it is with black being least discriminant and white being the most discriminant subband. The most discriminant subband represents the spatial frequency resolution that best discriminates between the meningioma subtypes under study. The subbands at those spatial frequency resolutions do not show much to the naked eye.

3.1 Stability for Subband Feature Selection

The selection of subbands from a given Full Wavelet Packet Decomposition based upon the discriminant function as employed in [1, 3, 17] is inherently a selection of features. Jain *et al.* presented a summary of all the various feature selection methods in [24] and found Sequential Features Selection as the best. Bhalerao and Rajpoot [25] described how wavelet based feature selection affects classification accuracies.

Stability has a direct impact on classification accuracy as it has an effect on feature selection. The more stable a subband, the more dependable it is for classification as it has been selected more often. In this paper, we use stability of the subbands in a decomposition to determine a mechanism for feature selection and derive a set of most probable discriminant features. This requires selecting the subbands that have maximum stability $\mathcal{S}_{d,p,q}$ which may be expressed as,

$$\mathcal{F}^*_{\mathcal{S}} = \{\mathcal{W}_{d,p,q} \in \mathcal{F}^* | \mathcal{S}_{d,p,q} = 1\} \tag{14}$$

where $\mathcal{F}^*_{\mathcal{S}}$ represents the set of most stable and discriminant subbands. A subband that is stable is inherently discriminant since the subband selection in ADWPT is based upon selecting the most discriminant subbands in an FWPT decomposition. Therefore, a subband which is selected in all decompositions for different texture data in the various trial runs has a relatively high discrimination power.

4 Results and Discussion

A leave-one-out mechanism was followed for classification of meningioma subtypes. At each trial four patients' data are left out (one belonging to each class) and the rest of the patients are used for training. There are 48 images per patient and using four patients data per meningioma subtype yields 192 images per subtype for training while 48 images per subtype are used for testing. After the

stability analysis, we have two choices: either to select all the subbands that are ever decomposed or only the ones that are decomposed always. For comparative purposes we first take a feature from each subband that is decomposed at least once and refer to them as all the subbands represented by feature set $\mathcal{F}^*$. We then select only the subbands that have mean frequency of occurrence of 1 and refer to them as the most stable subbands represented by $\mathcal{F}^*_{\mathcal{S}}$. Haralick's [26] Gray Level Co-occurrence Matrix (GLCM) based features are used over each subband to extract a feature set. The GLCM is computed in four directions i.e. 0^o 45^o, 90^o, 135^o while the distance remains as 1. The GLCM features were computed for various number of bins with 32 giving the best results. The results for 5-fold cross validation with one patient excluded per meningioma from the template construction and classification stage are presented in Table 1. Support Vector Machine (SVM) was the chosen classifier for the purpose and the Matlab version of LibSVM provided by Chang and Lin [27] was used in our analysis.

Test Trial #	Features	N	Acc_F	Acc_M	Acc_P	Acc_T	$Acc_{Overall}$
1	$\mathcal{F}^*$	247	65	83	94	73	79
	$\mathcal{F}^*_{\mathcal{S}}$	129	69	75	94	85	81
2	$\mathcal{F}^*$	247	92	98	100	75	91
	$\mathcal{F}^*_{\mathcal{S}}$	143	92	100	100	77	92
3	$\mathcal{F}^*$	244	83	67	100	92	85
	$\mathcal{F}^*_{\mathcal{S}}$	109	90	69	98	88	86
4	$\mathcal{F}^*$	244	67	100	96	94	89
	$\mathcal{F}^*_{\mathcal{S}}$	109	69	100	94	83	87
5	$\mathcal{F}^*$	244	88	98	98	88	93
	$\mathcal{F}^*_{\mathcal{S}}$	109	83	96	100	92	93
Avg	$\mathcal{F}^*$	245	79	**89**	97	84	87
(proposed)	$\mathcal{F}^*_{\mathcal{S}}$	120	80	**89**	97	**85**	**88**
Avg^*	$\mathcal{D}^*$ [1]	58	**91**	63	**99**	77	82

Table 1. Classification accuracy results for all four subtypes F=Fibroblastic, M=Meningiotheliamatous, P=Psammomatous and T=Transitional. N denotes the total number of features. Avg^* indicates the best cross validated results produced by Qureshi *et al.* [1] with the most discriminant subbands indicated by $\mathcal{D}^*$.

As can be seen from Table 1, the classification accuracy improves if the most stable subbands are used. Although the feature space is reduced greatly, the classification accuracies still improve. In comparison with the best results reported by Qureshi *et al.* [1], our results are improved but there is an increase in the number of subbands and the classification accuracies for the fibroblastic and psammomatous subtype fall but the results for meningiotheliamatous and transitional subtypes are greatly improved. The overall classification accuracy in our method is improved by 6%.

The Table 1 shows how the number of subbands selected change from all subbands to most stable subbands in the various test/trial runs. Although, the number of subbands selected falls by more than 50%, the classification accuracy improves in most cases. Hence, the improved and robust ADWPT offers a mechanism for overcoming the issue of data variability by obtaining a set of subband which represent significant textural characteristics that remain consistent even

when the data changes. Moreover, as can be seen from the results, the most stable subbands selected provide higher classification accuracies. Therefore, it can be safely concluded that the robust ADWPT is a good approach for texture classification in problems where high intra-class and low inter-class variation is found.

5 Conclusions

In this paper, we have presented a mechanism for obtaining a more robust ADWPT based representation that overcomes the issue of intra-class variability in histology images using the union of various decompositions. We show how subbands can be selected from the union set of subbands using stability as a measure. Although the feature space is reduced by 50% using our technique, the classification accuracies still improve, showing that the subbands selected using our novel stability based approach represent the textures under study better than the simple ADWPT. Moreover, it is shown that the novel robust ADWPT is a stable and efficient technique for classification of images for complex texture classification problems such as meningioma subtype classification.

An important factor that affects the classification accuracy is the discrimination power of the subbands whose features are included in the feature vector. When the most stable subbands are selected, in essence the most discriminant subbands are selected as well since these subbands were found to be highly discriminant in all the decompositions. However, in the most stable decomposition, lesser stable subbands are ignored. These can be included to see how they effect the classification accuracy. This would be the subject of future study.

Acknowledgements

The authors are grateful to Professor Roland Wilson for his support and ideas.

References

1. Qureshi, H., Sertel, O., Rajpoot, N., Wilson, R., Gurcan, M.: Adaptive discriminant wavelet packet transform and local binary patterns for meningioma subtype classification. In: Proceedings 11th Medical Image Computing and Computer-Assisted Intervention (MICCAI'2008). (2008)
2. Lessmann, B., Hans, V., Degenhard, A., Nattkemper, T.W.: Feature space exploration of pathology images using content-based database visualization. In: Proceedings SPIE Medical Imaging. (2006)
3. Qureshi, H., Rajpoot, N., Masood, K., Hans, V.: Classification of meningiomas using discriminant wavelet packets and learning vector quantization. In: Proceedings of Medical Image Understanding and Analysis. (2006)
4. Wirjadi, O., Breuel, T., Feiden, W., Kim, Y.J.: Automated feature selection for the classification of meningioma cell nuclei. In Handels, H., Ehrhardt, J., Horsch, A., Meinzer, H.P., Tolxdorff, T., eds.: Bildverarbeitung fr die Medizin. Informatik Aktuell, Springer (2006) 76–80
5. Naik, S., Doyle, S., Agner, S., Madabhushi, A., Feldman, M., Tomaszewski, J.: Automated gland and nuclei segmentation for grading of prostate and breast cancer histopathology. In: 5th IEEE International Symposium on Biomedical Imaging: From Nano to Macro (ISBI 2008). (May 2008) 284–287

6. Sahoo, P., Soltani, S., Wong, A.: Survey: a survey of thresholding techniques. Computer Vision Graphics Image Processing **41** (1988) 233–260
7. Francis, I., Adeyanju, M., George, S., Junaid, T., Luthra, U.: Manual versus image analysis estimation of pcna in breast carcinoma. Anal. Quant. Cytol. Histol. **22** (2000) 11–16
8. Petushi, S., Garcia, F.U., Haber, M.M., Katsinis, C., Tozeren, A.: Large-scale computations on histology images reveal grade-differentiating parameters for breast cancer. BMC Medical Imaging **6** (2006) 14
9. Ji, Q., Engel, J., Craine, E.: Texture analysis for classification of cervix lesions. IEEE Transactions on Medical Imaging **19**(11) (Nov. 2000) 1144–1149
10. Law, A.K.W., Lam, K.Y., Lam, F.K., Wong, T.K.W., Poon, J.L.S., Chan, F.H.Y.: Image analysis system for assessment of immunohistochemically stained proliferative marker (mib-1) in oesophageal squamous cell carcinoma. Computer Methods and Programs in Biomedicine **70**(1) (2003) 37 – 45
11. Schupp, S., Elmoataz, A., Fadili, J., Herlin, P., Bloyet, D.: Image segmentation via multiple active contour models and fuzzy clustering with biomedical applications. In: Proceedings. 15th International Conference on Pattern Recognition. Volume 1. (2000) 622–625 vol.1
12. M. Gurcan *et al.*: Histopathological image analysis: A review. Submitted to Medical Image Analysis (2009)
13. Demir, C., Gultekin, S., Yener, B.: Learning the topological properties of brain tumors. IEEE/ACM Transactions on Computational Biology and Bioinformatics **2**(3) (July-Sept. 2005) 262–270
14. Hamilton, P., Bartels, P., Thompson, D., Anderson, N., Montironi, R., Sloan, J.: Automated location of dysplastic fields in colorectal histology using image texture analysis. J. Pathol. **182** (1997) 68–75
15. Esgiar, A., Naguib, R., Sharif, B., Bennett, M., Murray, A.: Microscopic image analysis for quantitative measurement and feature identification of normal and cancerous colonic mucosa. IEEE Trans. Inf. Technol. Biomed. **2** (1998) 197–203
16. Gibson, D., Gaydecki, P.: Definition and application of a Fourier domain texture measure: applications to histological image analysis. Comput. Biol. Med. **25** (1995) 551–557
17. Qureshi, H., Wilson, R., Rajpoot, N.: Optimal wavelet basis for wavelet packets based meningioma subtype classification. In: Proceedings 12th Medical Image Understanding and Analysis (MIUA'2008). (2008)
18. Jafari-Khouzani, K., Soltanian-Zadeh, H.: Multiwavelet grading of pathological images of prostate. IEEE Transactions on Biomedical Engineering **50**(6) (2003) 697–704
19. Cross, S.: Fractals in pathology. J. Pathol. **182** (1997) 1–8
20. Cross, S., Bury, J., Silcocks, P., Stephenson, T., Cotton, D.: Fractal geometric analysis of colorectal polyps. J. Pathol. **172** (1994) 248–262
21. Cross, S., Howat, A., Stephenson, T., Cotton, D., Underwood, J.: Fractal geometric analysis of material from molar and non-molar pregnacies. J. Pathol. **173** (1994) 115–118
22. Julesz, B., Bergen, J.R.: Textons, the fundamental elements in preattentive vision and perception of textures. Morgan Kaufmann Publishers Inc., San Francisco, CA, USA (1987)
23. Coifman, R.R., Wickerhauser, M.V.: Entropy-based algorithms for best basis selection. IEEE Transactions on Information Theory **38**(2) (1992) 713–718
24. Jain, A., Zongker, D.: Feature selection: Evaluation, application, and small sample performance. IEEE Trans. Pattern Anal. Mach. Intell. **19**(2) (1997) 153–158
25. Bhalerao, A., Rajpoot, N.: Discriminant feature selection for texture classification. In: Proceedings British Machine Vision Conference (BMVC'2003). (2003)
26. Haralick, R., Shanmugan, K., Dinstein, J.: Textural features for image classification. IEEE Trans. Syst. Man Cybern. **3** (1973) 610–621
27. Chang, C.C., Lin, C.J.: LIBSVM: a library for support vector machines. (2001) Software available at urlhttp://www.csie.ntu.edu.tw/c̃jlin/libsvm.

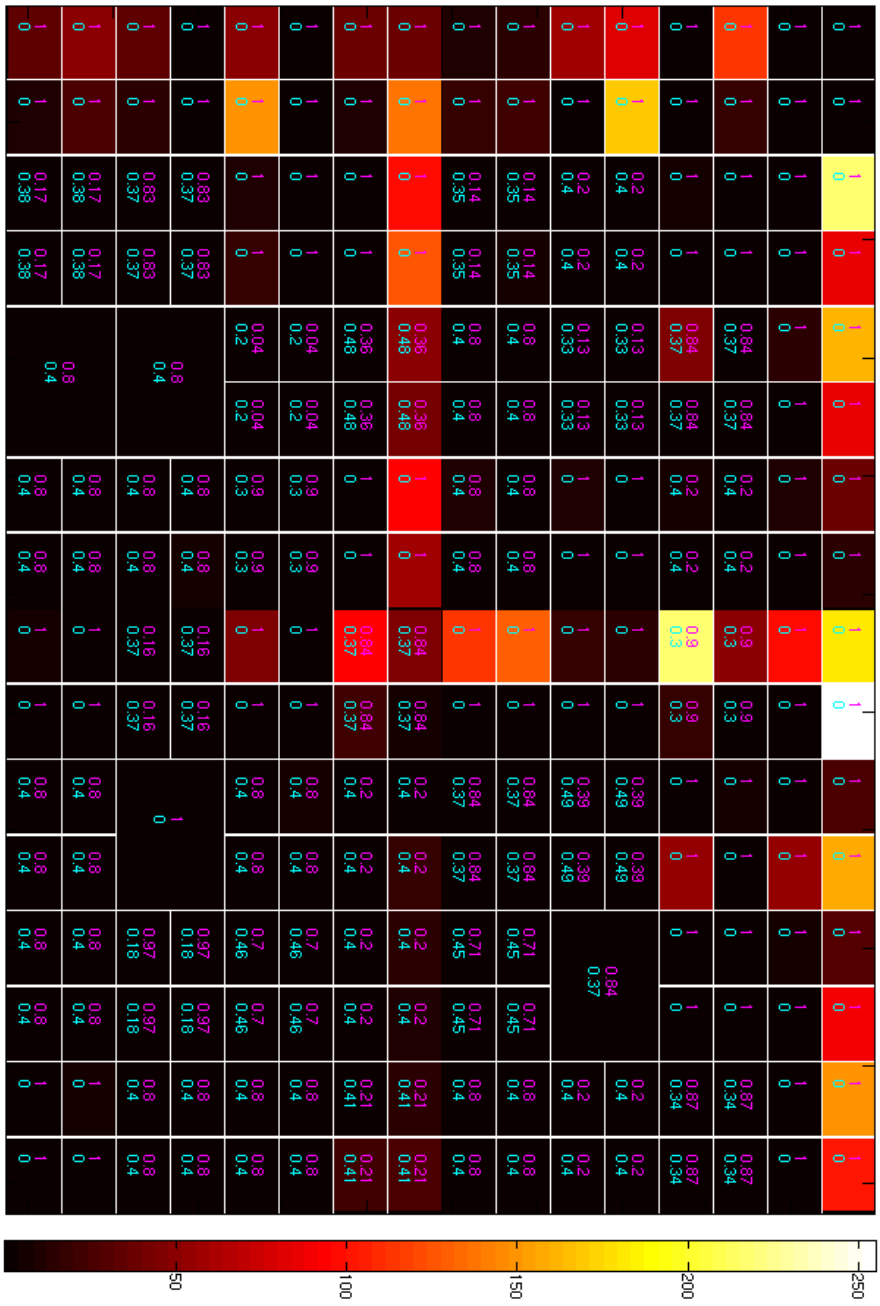

Fig. 4. Stability of the subbands in a union decomposition of 256 ADWPT decompositions obtained using the Fisher Distance (the lighter the subband the more discriminant)